Aromatic Porous Polymer Network Membranes for Organic Solvent Nanofiltration under Extreme Conditions

Journal:	*Journal of Materials Chemistry A*
Manuscript ID	TA-ART-09-2019-010190.R1
Article Type:	Paper
Date Submitted by the Author:	06-Nov-2019
Complete List of Authors:	Wang, Chenxu; Texas A&M University, Materials Science & Engineering Li, Chenxuan; Texas A&M University, Chemistry Rutledge, Evan; Texas A&M University, Chemistry Che, Sai; Texas A and M University System Lee, Jongbok; University of California Santa Barbara, Materials Research Laboratory Kalin, Alexander; Texas A&M University College Station, Zhang, Caili; Beijing Technology and Business University, Zhou, Hong-Cai; Texas A&M University, Chemistry Guo, Zi-Hao; South China University of Technology, South China Advanced Institute for Soft Matter Science and Technology, School of Molecular Science and Engineering Fang, Lei; Texas A&M University, Chemistry; Texas A&M University, Materials Science and Engineering

ARTICLE

Aromatic porous polymer network membranes for organic solvent nanofiltration under extreme conditions

Chenxu Wang,[ab] Chenxuan Li,[a] Evan R. C. Rutledge,[a] Sai Che,[a] Jongbok Lee,[a] Alexander J. Kalin,[a] Caili Zhang,[a] Hong-Cai Zhou,[ab] Zi-Hao Guo*[c] and Lei Fang*[ab]

Aromatic porous polymer networks (PPNs) are promising candidate materials for organic solvent nanofiltration (OSN) membranes, in which molecular-sieving selectivity, high permeability, and chemical/structural stability can be integrated. In this work, aromatic PPN membranes *p*-PPN, *m*-PPN and *tri*-PPN are fabricated by *in situ* aldol triple condensation cross-linking. These membranes demonstrate high stability, permeability and sharp selectivity in OSN, thanks to the aromatic nature of the backbone, high surface area (up to 1235 m²/g), and narrowly distributed pore sizes. They possess a high organic solvent permeability so that a good permeance is achieved despite a thickness over 100 μm. Molecular weight cut-off and molecular weight retention onset of these membranes are ~600 g/mol and 350 g/mol, respectively, making it possible to efficiently separate molecules from a complex mixture composed of compounds with only marginally different molecular weights. As a result of the highly stable nature of the aromatic backbones, these PPN membranes show retained structural integrity and OSN performance in the presence of either strong acid or strong base for over 50 h. The extraordinary stability, integrated with the excellent permeability and selectivity, render these PPN membranes promising candidate for challenging OSN applications under extreme conditions.

Introduction

Organic solvent nanofiltration (OSN) through membranes have emerged as an environmentally and energetically favorable strategy to purify, separate, and concentrate organic solutions for a wide range of applications.[1-5] To date, various types of membranes, including polymeric, inorganic and mixed matrix membranes, have been developed for OSN.[1-3, 6-9] Among them, polymeric membranes[10, 11], especially those ones with high permeability and selectivity[12, 13], are particularly promising due to their feasible manufacturing, mechanical adaptability, and synthetic versatility. Most commercial polymeric membranes for OSN are dense membranes with little or no porosity[1, 13] and usually suffer from low permeability. Moreover, their non-cross-linked nature also lowers their resistance to strong organic solvents or harsh chemical environments.[14, 15] In contrast, cross-linked porous polymeric membranes are promising in terms of permeability because of the presence of interconnected pores and channels which assist molecular transportation.[13] Cross-linked membranes also exhibit desired solvent resistance compared to non-cross-linked alternatives.[16, 17] In addition, recently developed crystalline covalent organic framework (COF) membranes, which are covalently cross-linked and highly porous, have shown excellent selectivity and extraordinary permeance in OSN with various solvents on account of the long range order of their pore structures.[18-23] In comparison, an amorphous cross-linked porous polymer network (PPN) can be prepared via a wide range of synthetic methods, creating a diverse library of PPNs with different cross-linking chemistries and backbone constitutions.[24-29] A number of high-performance, PPN-derived OSN membranes have been successfully developed, including polyarylate membranes[30], cyclodextrin membranes[31, 32], and conjugated microporous polymer (CMP) membranes.[33, 34]

Despite the significant advances in the field of polymeric OSN membranes, it is still a formidable challenge to achieve an ideal polymeric membrane possessing simultaneously chemical/structural stability, molecular-sieving selectivity, and high permeability/permeance. In particular, the performance and structural integrity of most polymer membranes tend to decline rapidly in harsh chemical environments, which are often unavoidable in practical applications.[1, 2, 35-37] Many of the key chemical bonds in polymeric membranes (such as ester bonds, imine bonds) are labile in strong acidic or basic conditions. Highly permeable and selective polymeric OSN membranes that can perform reliably with chemically aggressive feeds are still extremely rare. In order to achieve a stable, selective, and permeable membrane for OSN, one must simultaneously impart good chemical stability, high porosity, and narrow pore size distribution into polymeric OSN membranes.[35, 38, 39] We hypothesized that organic membranes constituted of a fully aromatic network could potentially fulfil these demands.

[a] *Department of Chemistry, Texas A&M University, 3255 TAMU, College Station, Texas 77843, USA. E-mail: fang@chem.tamu.edu*
[b] *Department of Materials Science and Engineering, Texas A&M University, 3003 TAMU, College Station, Texas 77843, USA. E-mail: fang@chem.tamu.edu*
[c] *South China Advanced Institute for Soft Matter Science and Technology, South China University of Technology, Guangzhou 510640, China. E-mail: guozihao@scut.edu.cn*

Herein, we report the fabrication of a class of aromatic PPN membranes possessing extraordinary stability, excellent permeability and molecular-sieving selectivity, as well as highly robust OSN performance in strong acid and base conditions.

Experimental

Fabrication of PPN thin films

The commercially available monomer (1,4-diacetylbenzene, 1,3-diacetylbenzene or 1,3,5-triacetylbenzene) was dissolved in methanesulfonic acid (MSA) at 50 °C to form a 15 mg/mL solution. The solution was drop casted onto a micro cover glass and sandwiched by another micro cover glass, followed by heating at 110 °C for 24 h. After the reaction was completed, the micro cover glasses were separated and the PPN film was adhered to one of the glass pieces. A pressure-sensitive tape was used to tape off the film from the glass surface (Figure S1). The tape was then soaked in THF where the polyacrylate adhesive was dissolved and PPN thin film was released into THF, and subsequently transferred onto a silicon wafer by using a pipette, and rinsed with THF for further tests.

Fabrication of PPN membranes for OSN.

The monomer (90 mg) was dissolved in MSA (1 mL) at 50 °C to form the reaction solution. The solution was drop casted onto a 6" × 6" glass substrate and sandwiched between another piece of glass of the same size. These glass substrates were pre-treated by spray-coating a thin layer of PTFE to prevent undesired adhesion of the membrane onto the glass. Two pieces of 200 μm-thick micro cover glass slides were placed in between (Figure 1b). The sandwiched system was heated at 110 °C for 24 h. After the reaction, the freestanding PPN membrane was detached from the glass substrate and soaked in methanol for 45 min. It was then taken out and soaked in another batch of clean methanol. After repeating for twice, the membrane was either used directly for subsequent experiments, or preserved by soaking in PEG 600/methanol solution (weight ratio = 1:1) overnight and dry in the air for long-term storage. In order to determine the yield, the membrane was first grounded into powder, washed thoroughly by Soxhlet extraction with THF, and subsequently dried to give the precise mass.

OSN tests of PPN membranes.

A piece of PPN membrane was washed thoroughly with methanol and cut by a round cutter with diameter of 4.7 cm. The membrane was transferred into a dead-end solvent-resistant stirred cell (Millipore, effective diameter 4.7 cm) with a Nylon filtration membrane (Whatman, 0.45 μm pore size) underneath as a cushion (Figure S2). A Kalrez® solvent-resistant O-ring (outside diameter 4.7 cm) was placed on the PPN membrane to seal the cell. All experiments were repeated at least three times. In a typical dye rejection test, dye solution (30 mL, 10 ppm) was charged into the cell as the feed solution. A transmembrane pressure of 1 bar was applied by using compressed nitrogen gas. The feed solution was stirred at 400 rpm to minimize concentration polarization effect close to the membrane. The first 3 mL of permeate was discarded and the following permeate was collected for measurements. After the test, the solution remained in the cell was collected as the retentate. The concentration of feed, permeate, and retentate was measured by UV-vis spectrophotometer. The rejection R was calculated using Equation (1), where C_f and C_p is the concentration of feed and permeate, respectively.

$$R = \left[1 - \left(\frac{C_p}{C_f} \right) \right] \times 100\% \quad (1)$$

In pure solvent permeance tests, 30 mL pure organic solvent (acetonitrile, acetone, methanol, tetrahydrofuran, toluene, dimethylformamide, or isopropanol) was used as the feed. The permeation test was conducted under transmembrane pressure of 1 bar with stirring rate of 400 rpm. The first 3 mL was discarded and the permeation time and solvent volume of the following permeate was recorded. The permeance p of PPN membrane was calculated using Equation (2), where V is solvent volume, A is effective area of membrane, t is time, Δp is TMP.

$$p = \frac{V}{A.t.\Delta p} \quad [unit: L\ m^{-2}\ h^{-1}\ bar^{-1}] \quad (2)$$

The permeability P, which reveals the intrinsic property of materials, of PPN membrane was calculated using Equation (3), where p is permeance and l is the thickness of membrane.

$$P = pl \quad [unit: L\ m^{-2}\ h^{-1}\ bar^{-1}\ m] \quad (3)$$

In mixed dye separation test where rhodamine B was separated, a mixture of 2.5 ppm rhodamine B, 15 ppm bromothymol blue, 15 ppm congo red, and 10 ppm brilliant blue in methanol were used as the feed solution. Different concentrations of the dyes were used in order to avoid overwhelming signal intensity of one certain dye, so that the absorption signals in the UV-vis spectra were easy to deconvolute during analysis. In mixed dye separation test where fluorescein and rhodamine B were separated, the concentration of fluorescein, rhodamine B and bromothymol blue were all 10 ppm in methanol. In order to differentiate peaks of fluorescein and bromothymol blue, NaOH was added into the feed solution to shift the peak of bromothymol blue.

Results and discussion

Fabrication of PPN membranes

The PPN membranes reported in this work are fabricated by cross-linking using an aldol triple condensation (ATC) reaction. In our previous work, a feasible ATC method based on methanesulfonic acid (MSA) was developed to efficiently produce amorphous aromatic PPNs in the form of powders with high porosity.[40] In this reaction, MSA acted as both the catalyst and the solvent so that no other reagent is needed for the "pristine" cross-linking. We envisioned that this unique feature could allow for fabrication of PPN membranes through an *in situ* cross-linking procedure using MSA as the solvent. It is also noteworthy that small amount of reaction defects, such as unreacted acetyl groups and α,β-unsaturated ketone units, are unavoidable in the product due to the less than 100% conversion and irreversible nature of the ATC reaction.[41] Based on this reaction, *p*-PPN, *m*-PPN, and *tri*-PPN membranes were
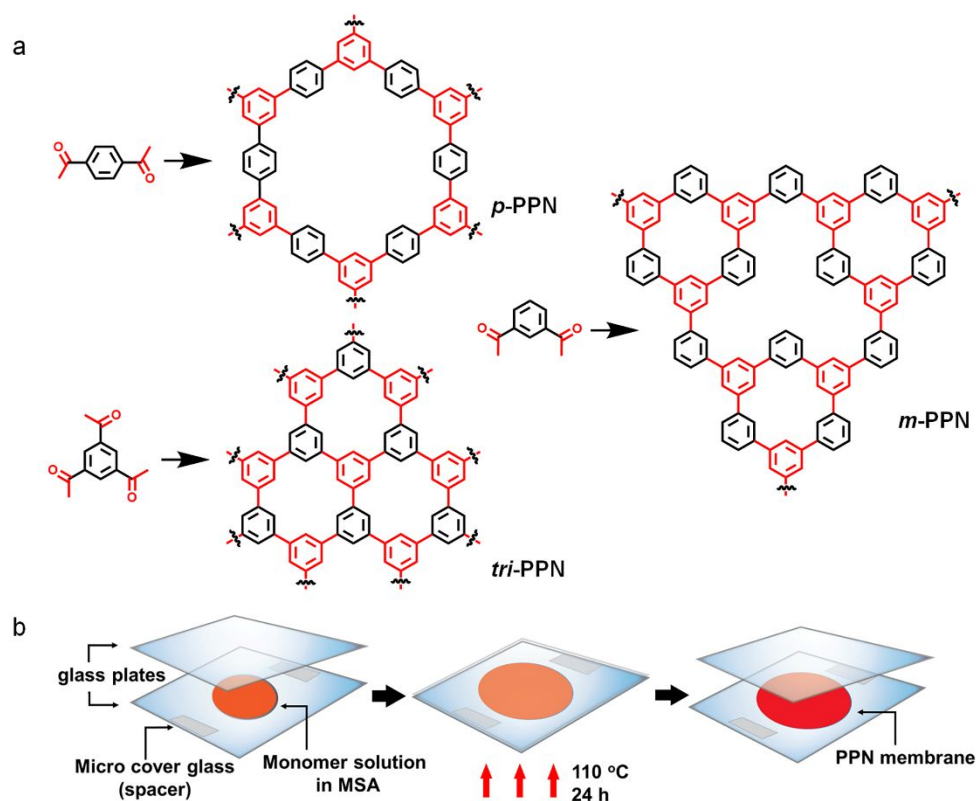
Figure 1. a) Synthetic scheme of cross-linked conjugated PPNs (*p*-PPN, *m*-PPN, and *tri*-PPN) through aldol triple condensation reaction; b) Graphic representation of the membrane fabrication using an MSA solution of the monomer.

fabricated using pristine solutions of 1,4-diacetylbenzene, 1,3-diacetylbenzene or 1,3,5-triacetylbenzene in MSA solvent, respectively (Figure 1a). These benzene-derived monomers are all commercially available. They were selected so that the ATC reaction led to PPNs with aromatic backbone with the desired stability and rigid microporosity. The different substitute patterns of para-, meta- and tri-acetyl functionalized monomers allows for the construction of variable pore structures. The reaction yields for *p*-PPN, *m*-PPN, and *tri*-PPN membranes were 88%, 84% and 91%, respectively.

A series of PPN membranes with different thicknesses, ranging from 150 nm to 120 μm, were prepared by this method with excellent quality. The membrane thickness was simply controlled by tuning the concentration of the initial monomer solution and the thickness of the spacer. For example, a membrane with sub-micrometer thickness was prepared from a 15 mg/mL monomer solution with no spacer between the two glass slides. After the heating process, the as-prepared membrane was removed from the glass slide with adhesive tape and separated from the tape by soaking in THF. The resulting free-standing membrane floats on the surface of the THF and can be picked up by a copper wired loop (Figure 2a). The freestanding PPN membrane was transferred onto a silicon wafer for atomic force microscopy (AFM) and scanning electron microscopy (SEM) characterization. The surface of these membranes have RMS roughnesses ranging from 15.9 nm to 19.1 nm (Figure 2b, Figure 2e Figure S4 and Table S1), which is similar to other PPN membranes prepared by surface-initiated

method[33] but smaller than COF membranes obtained from drop-casting method[18]. AFM height profiles (Figure 2c and Figure S3) show that the thicknesses of *p*-PPN, *m*-PPN, and *tri*-PPN prepared by this method are around 150-200 nm (Figure 2f and Figure S3). These thin membranes appeared to be highly flexible and able to crumple and fold on the wafer as visualized by SEM (Figure 2d). The thickness of the membrane can be controlled simply by tuning the concentration of the monomer solution. For example, when using a 30 mg/mL 1,3,5-triacetylbenzene solution for the process, it afforded a *tri*-PPN membrane with 360 nm thickness (Figure S5). Although these sub-micrometer-thick membranes were too fragile and small to be tested in a centimetre-sized OSN device, the successful synthesis demonstrated here proves the concept of *in situ* cross-linking method for the fabrication of conjugated PPN membranes for various application, including OSN.

In order to fabricate PPN membranes with adequate mechanical strength and size that can be feasibly handled for OSN in a 4.7-cm-diameter cell, higher concentration monomer solutions (90 mg/mL) and 200 μm-thick glass spacers were used to prepare a series of much thicker and larger membranes (5~6 cm in diameter), which can be easily peeled from the glass slides without the assistance of tape. The surface morphology of these membranes was smooth and unremarkable, while the cross-section image did not show any observable unsymmetrical feature (Figure 2h, 2i, and Figure S6). According to cross-section SEM images, the thicknesses of the *p*-PPN, *m*-PPN, and *tri*-PPN membranes were 121 ± 12, 118 ± 20, and 102 ± 19 μm,
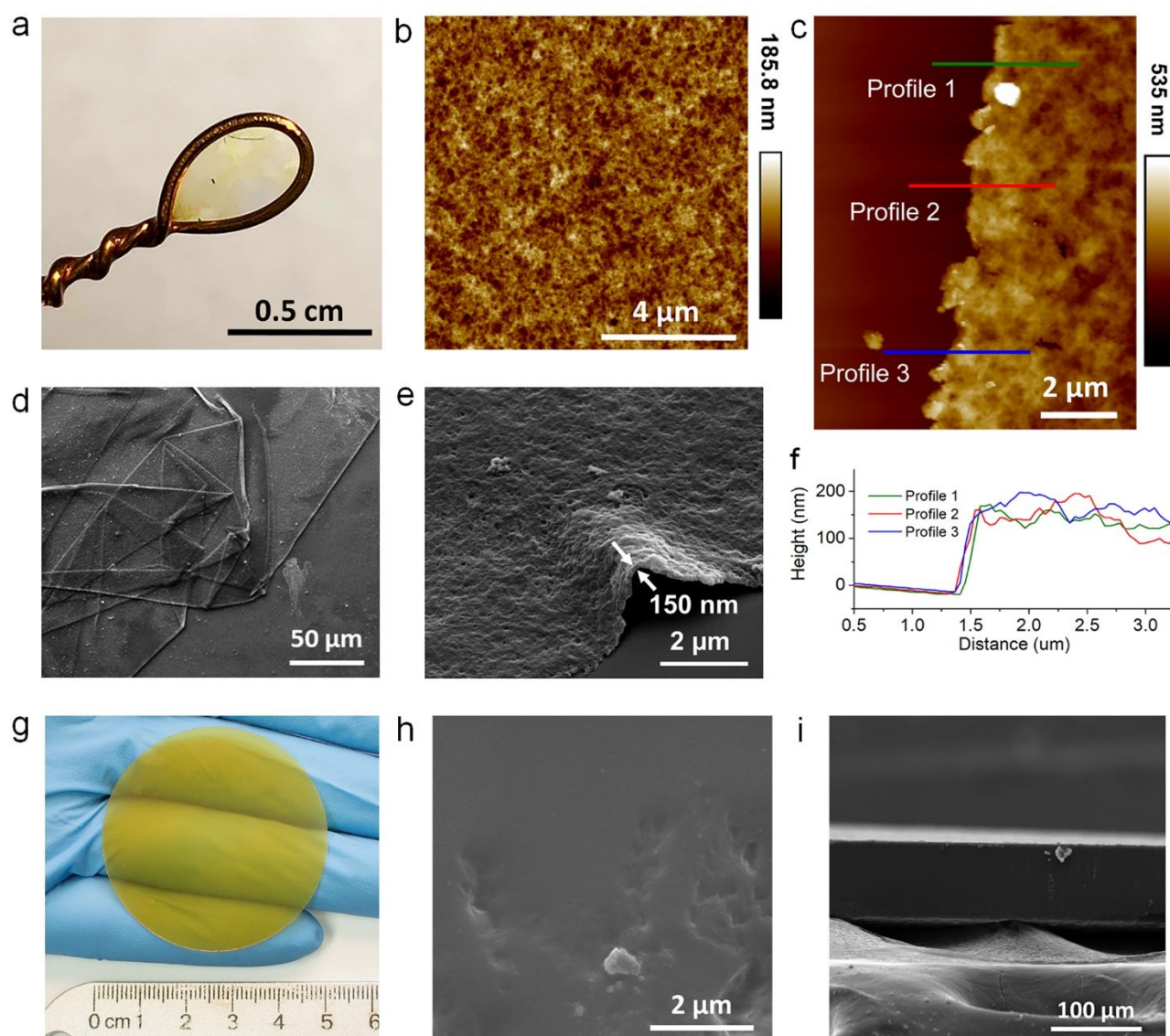
Figure 2. a) photographic image of a free-standing thin *tri*-PPN membrane with ~200 nm thickness on a copper loop; b,c,f) AFM images showing the surface morphology and thickness of the thin *tri*-PPN membrane; d,e) SEM images showing the flexible nature and the cross section of the thin *tri*-PPN membrane. g) photographic image of a thick *p*-PPN membrane for OSN with thickness of ~100 μm; h,i) SEM images of the surface and cross-section view of the thick *p*-PPN membrane.

respectively. They were washed with methanol and subsequently preserved with polyethylene glycol (PEG) 600 to prevent over-drying. These easy-to-handle, free-standing PPN membranes were cut into round pieces with diameter of 4.7 cm for further OSN measurements (Figure 2g and Figure S7). Contact angle tests showed the hydrophobic nature of PPN membranes (Figure S8).

Characterization

Chemical characterization of these PPN membranes were performed by using Fourier-transform infrared spectroscopy (FTIR) and solid-state ^{13}C CP/MAS nuclear magnetic resonance (SSNMR) (Figure 3a and 3b). FTIR spectra of these membranes were identical to the corresponding powder samples as reported previously.[40] As anticipated, the finger print feature of a 1,4-disubstituted benzene ring at 825 cm^{-1} was observed in the spectrum of *p*-PPN, while that of 1,3-disubstituted benzene ring at 790 cm^{-1} was identified in that of *m*-PPN. In addition, the characteristic features of 1,3,5-trisubstituted benzene rings at 858 – 879 cm^{-1} and 700 cm^{-1} were observed in all of these spectra. FTIR peaks corresponding to aromatic alkenes at 1577 - 1600 cm^{-1} and carbonyl groups at 1670 - 1707 cm^{-1} were also observed (Figure S9), indicating the presence of functional group defects resulting from incomplete conversion of the ATC reaction. In the SSNMR spectra, the sp^2 carbons substituted with hydrogen and those without hydrogen can be distinguished into two major resonance signals at 124.6 – 126.9 ppm and 140.7 ppm, respectively. Notably, in *p*-PPN and *m*-PPN, the ratio of signal intensities between the hydrogen
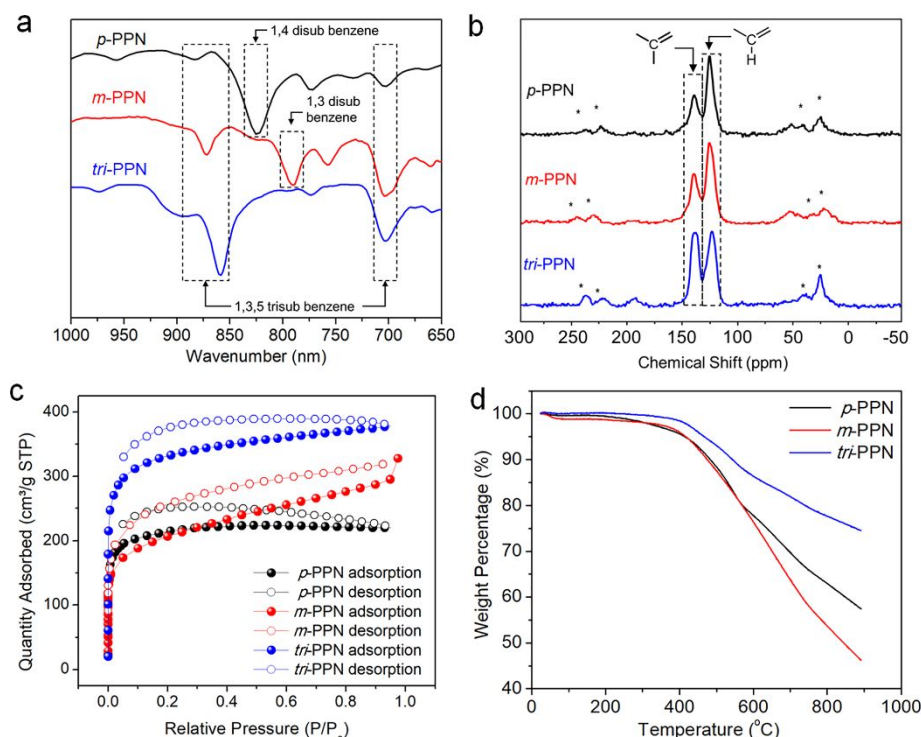
Figure 3. Characterization data of *p*-PPN, *m*-PPN, and *tri*-PPN membranes: a) Aromatic fingerprint region of FTIR spectra; b) SSNMR spectra; c) N$_2$ adsorption isotherms; d) TGA traces.

substituted carbons and the non-hydrogen carbons were similar and significantly higher than that in *tri*-PPN, in accordance to the theoretical compositions of these different types of carbons in the products. The amorphous structure of PPN membranes was confirmed by powder X-ray diffraction tests where no distinct diffraction peak was observed (Figure S10).

The porosity of these PPN membranes was characterized by N$_2$ adsorption tests at 77 K. The N$_2$ adsorption data showed type I isotherms, revealing microporosity in the PPN membranes (Figure 3c), similar to the corresponding powder samples[40]. Despite their amorphous nature and defects, these PPN membranes showed narrowly distributed pore sizes with a majority of the pores smaller than 1.5 nm (Figure S11). Particularly, *p*-PPN showed a major peak at 1.2 nm in the pore size distribution diagram, in agreement with the estimated pore size from the ideal structure shown in Figure 1a and Figure S12. The measured pore sizes of m-PPN and tri-PPN, however, were slightly larger than the estimated values, likely a result of more defects on the sterically demanding backbone around the smaller pores. Nevertheless, *tri*-PPN, composed of only tri-substituted benzene rings, exhibited the smallest average pore size among these samples. The major peak in pore size distribution diagram of *tri*-PPN is located at 0.6 nm. Also as expected, broader pore size distribution of *m*-PPN was observed with the major peak ranging from 0.7 nm to 1.2 nm resulting from the less symmetrical 1,3-disubstituted monomer. The Brunauer-Emmett-Teller (BET) surface areas of *p*-PPN, *m*-PPN, and *tri*-PPN membranes were determined to be 802, 734, and 1235 m^2/g, respectively (Table S2). The BET surface area of *p*-PPN membrane was also close to that of the bulk powder

sample of *p*-PPN[40], indicating the high efficiency of the *in situ* ATC cross-linking reaction in the membrane. Benefiting from the rigid framework, *tri*-PPN demonstrated a high BET surface area compared to CMP membranes with similar pore size.[33] The thermal stability of PPN membranes was characterized by thermogravimetric analysis (TGA, Figure 3d). The 5% weight loss onset temperatures for *p*-PPN, *m*-PPN, and *tri*-PPN were all above 410 $^\circ$C. Especially, *tri*-PPN was stable with less than 10% weight loss until 543 $^\circ$C. The outstanding thermal stability of these PPN membranes can be attributed to the aromatic nature of the backbone. It enables potential application of these membranes in some high temperature conditions that were conventionally only possible with ceramic membranes.[42]

Organic Solvent Nanofiltration Performance

With high porosity and narrowly distributed pore size, *p*-PPN and *tri*-PPN membranes were expected to possess high permeability and good selectivity for efficient OSN. To test their OSN performances, pinhole-free PPN membranes with thickness around 100 μm and diameter of 4.7 cm were tested by using a dead-end solvent resistant stirred cell (Figure S2). Methanol solutions of various organic dyes, with molecular weight ranging from 332 g/mol to 1017 g/mol to meet the nanofiltration requirements (200-1000 g/mol), were used as feed solutions to be filtered through the membranes under a transmembrane pressure (TMP) of 1 bar. The dyes used are fluorescein, rhodamine B, bromothymol blue, congo red, brilliant blue, and rose bengal (see Table S3 for chemical structures and molecular sizes). The rejection rate of PPN membranes to each dye was defined as the percentage ratio of
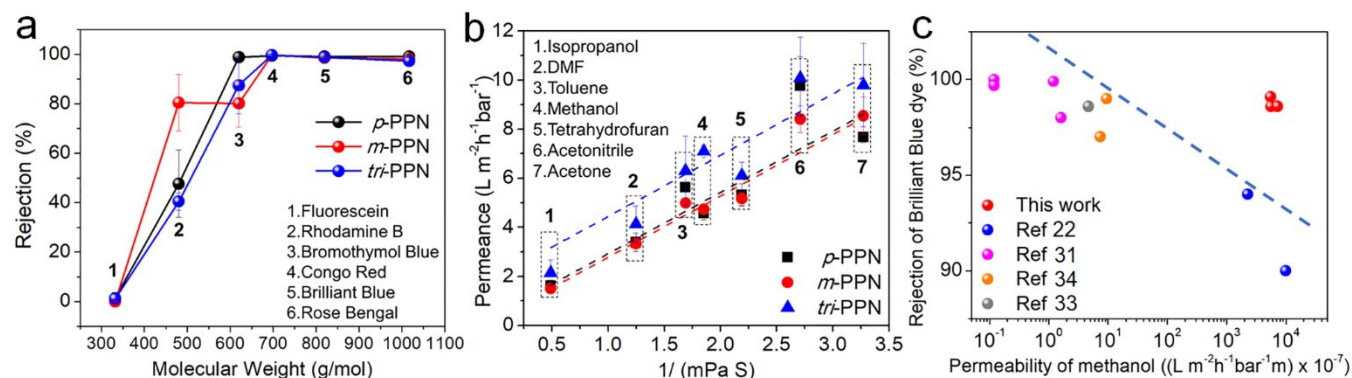
Figure 4. OSN performance of *p*-PPN, *m*-PPN, *tri*-PPN membranes: a) Rejection rate as a function of the molecular weight of the dye solute; b) Membrane permeance values as a function of the solvent viscosity; c) Rejection of brilliant blue verses permeability of methanol for PPN membranes, comparing with reported microporous polymer membranes, including COFs, polyarylate, CMPs, and cyclodextrin. The dash line indicates an upper bond.

the concentration between the permeate and the feed solutions compared with the original feed concentration, all measured by UV-vis absorption spectroscopy following the Beer-Lambert law (Figure S13). The rejection rates were plotted against the molecular weights of the dyes (Figure 4a). As expected, *p*-PPN, *m*-PPN, and *tri*-PPN membranes showed almost complete rejection (98 – 99.7%) to larger dyes such as congo red (687 g/mol), brilliant blue (820 g/mol) and rose bengal (1017 g/mol). Neutral compound bromothymol blue (624 g/mol) was also completely rejected by *p*-PPN membranes. Considering the charge-neutral and non-polar nature of the backbone as well as the negligible electrostatic repulsion/interaction between the solute molecules and the membrane backbone in organic solvent,[20] the rejection mechanism was attributed to size exclusion instead of charge repulsion or polar interaction. The molecular weight cut-off (MWCO) of *p*-PPN, *m*-PPN, and *tri*-PPN membranes were approximately 600, 660, and 630 g/mol, respectively, which are similar to those of CMP membranes with similar pore size.[33] The rejection rate decreased drastically as the molecular weight of the dyes decreased. The molecular weight retention onset (MWRO), where the rejection is 10%, of all the PPN membranes were around 350 g/mol. Selectivity measured based on MWRO and MWCO of *p*-PPN and *tri*-PPN membranes are comparable to those of highly crystalline COF membranes[20]. Such a good selectivity was attributed to the narrowly distributed pore sizes of the PPN membranes. It is also noteworthy that *m*-PPN membrane showed an anticipated lower selectivity, a result of its broader pore size distribution. It is also noteworthy that the adsorption of the dye molecules to the membrane was possible[43-45] but was not significant at the concentration used in the OSN experiments, indicated by the comparable concentration of the permeated small dyes and increased concentration of the rejected retentate (Figure S12).

The sharp OSN selectivity allowed for efficient separation of organic compounds that are only moderately different from each other in size, which has been a challenging task for membrane separation. For example, in a test of separating a complex mixture of four dyes, rhodamine B (479 g/mol) can be isolated efficiently from bromothymol blue (624 g/mol), congo red (697 g/mol) and brilliant blue (820 g/mol) through a p-PPN membrane (Figure 5a). After a standard OSN operation of the feed solution containing the aforementioned four dyes, the permeate solution contained only rhodamine B while the three larger dyes were rejected. The UV-vis spectrum of the permeate showed that the absorption peak of bromothymol blue at 620 nm was completely removed after OSN. Similarly, in another OSN test of a three-dye mixture of fluorescein, rhodamine B and bromothymol blue, only bromothymol blue (624 g/mol) was rejected by p-PPN membrane while the smaller dyes fluorescein (332 g/mol) and rhodamine B (479 g/mol) permeated (Figure 5b). By using this method, dyes smaller than the MWCO could be separated from dyes larger than the MWCO in mixed solutions in a highly efficient manner without tedious chromatography, demonstrating the advantages of using microporous membrane to perform size-selective OSN separation over the conventional dense membrane of which separation mainly depends on different permeability and diffusivity.[13]

The cross-linked network and the aromatic hydrocarbon backbone make these PPN membranes suitable for OSN of a wide range of organic solvents, including nonpolar, polar aprotic, and polar protic solvents. Permeance of a wide range of organic solvents through these membranes (Figure S12) was found to be linearly related with the reciprocal of solvent viscosity, but not correlated with molecular diameter, solubility parameter or dielectric constant (Figure 4b, Figure S14), suggesting that the diffusion of solvent through these PPN membranes followed a pore flow model.[46, 47] It also indicated that solvent permeance was not significantly impacted by possible chemical interaction of the solvent molecules with the membrane backbone or with the defect sites.[20] The pressure normalized permeance of methanol, toluene, and THF all remained constant under different TMPs (Figure S15). The permeance of *tri*-PPN membrane was consistently higher than that of *p*-PPN and *m*-PPN membranes, benefitting from its
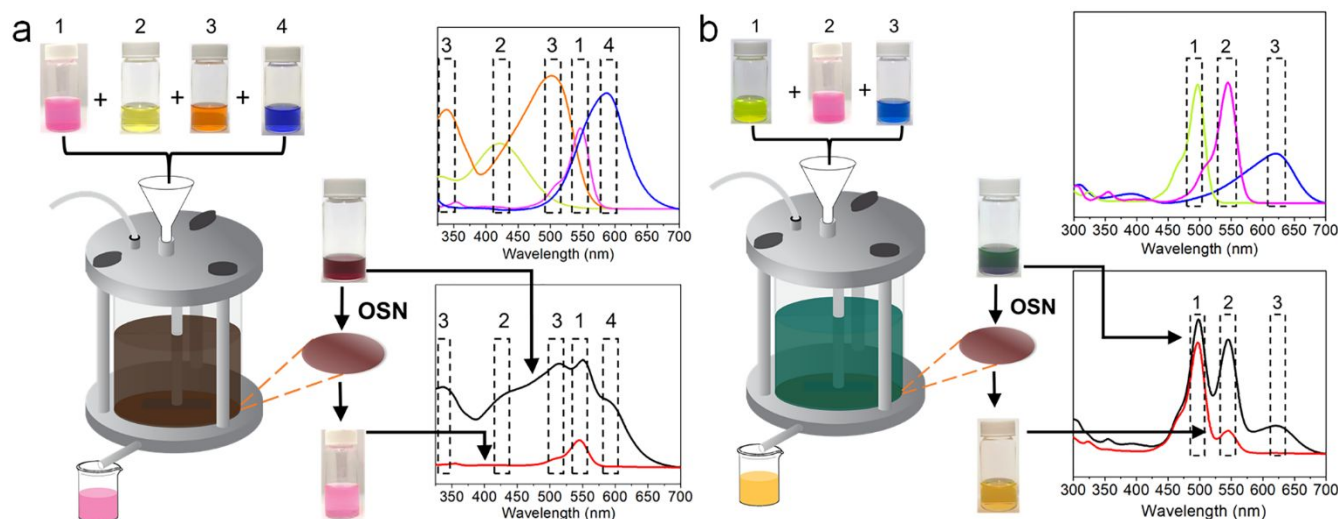
ARTICLE

Figure 5. Scheme of dye separation performance of p-PPN membrane and UV-vis absorption spectra of the feed solution and the permeate: a) Separating (1) rhodamine B from (2) bromothymol blue, (3) congo red and (4) brilliant blue; b) Separating (1) fluorescein and (2) rhodamine B from (3) bromothymol blue.

higher porosity. Notably, the permeance of toluene for these PPN membranes (5 – 6.3 L m^{-2} h^{-1} bar^{-1}) was higher than that of CMP membranes (4.2 L m^{-2} h^{-1} bar^{-1})[33] with similar MWCO even though these measured PPN membranes were much larger in size and three orders of magnitude thicker. The intrinsic permeability values of methanol through p-PPN, m-PPN, and tri-PPN were 5.53 x 10^{-4}, 5.593 x 10^{-4}, and 7.242 x 10^{-4} L m^{-2} h^{-1} bar^{-1} m, respectively, significantly higher than many benchmark polymeric OSN membranes.[12] For microporous polymer membranes, the permeability typically remains constant from thicknesses between 100 nm and 30 μm with a TMP as high as 15 bar.[17] The rejection performance against brilliant blue (a widely studied model dye for OSN) and permeability of these PPN membranes in methanol are plotted in comparison with those of representative cohorts of polymeric OSN membranes (Figure 4c, Table S4). These literature examples including membrane of COFs,[21] polyarylate,[30] conjugated microporous polymers,[33] and cyclodextrin[32]. The plot showed a trade-off relationship between permeability and selectivity, so that an upper bound was observed.[48, 49] Compared with these literature data, the PPN membranes in this work are situated well above the upper bound with excellent solvent permeability while maintaining a high solute rejection rate. This remarkable combination of properties was attributed to the highly porous and non-interactive nature of the aromatic backbone of these PPN membranes.

Stability Test

The rigid cross-linked aromatic framework also imparted the PPN membranes with extraordinary chemical stability and robust porous structure, which is critical for OSN performance in extreme conditions. The stability of aromatic PPN membranes were studied extensively. First, p-PPN membranes were soaked in a variety of solutions with harsh conditions for 5 days: 18 M H_2SO_4, 0.1 M chromic acid, 14 M NaOH in water/methanol, and 2 M $NaBH_4$ in methanol. FTIR spectra of

these treated samples all showed similar peak positions and retained features for 1,4- and 1,3,5-substituted benzene rings, indicating that the PPN backbone was mostly intact during these treatments. Minor changes on certain IR peaks were observed on the samples treated with $NaBH_4$, H_2SO_4 and chromic acid, likely a result of reduction or oxidation of the residual defect sites (e.g., the ketone and α,β-unsaturated ketone groups). (Figure S16). The surface morphology of those PPN membranes were also maintained well after these treatments according to SEM (Figure S17). OSN of p-PPN membranes after soaking in 18 M H_2SO_4 and in 5 M NaOMe in methanol for 2 days were investigated. The rejection of congo red and rose bengal of these treated p-PPN membranes remained at 99.0% and 98.2%, respectively (Figure S18). Long-term OSN performance of p-PPN membrane under harsh conditions was examined through OSN of strong acid and strong
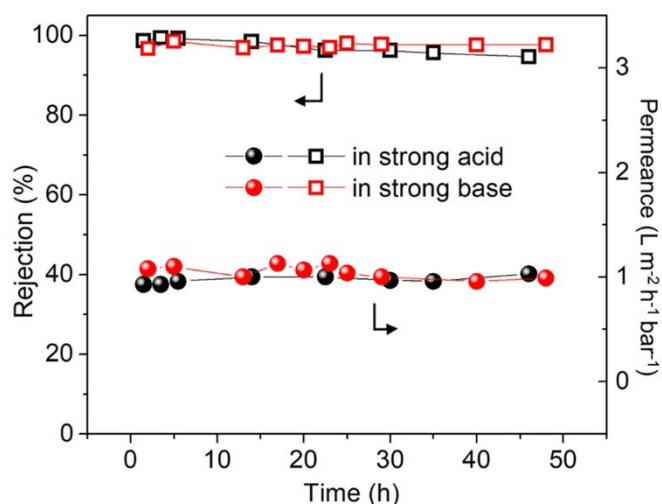

Figure 6. Long-term OSN test of p-PPN membrane filtrating isopropanol solutions of brilliant blue in the presence of PTSA and rose bengal in the presence of NaOH.

base solutions for 48 h. Specifically, brilliant blue in isopropanol with 10 mM p-toluenesulfonic acid (PTSA) was used to test acidic condition, while rose bengal in isopropanol with 10 mM NaOH was used for basic conditions. In both cases, the rejection of the dye remained over 95% and the permeance of isopropanol was steady over 48 h (Figure 6). Similarly, stable performance was also observed on smaller dyes such as congo red in ethanol (Figure S19). Such a remarkable stability outperforms most commercial organic OSN membranes[50-52] (Table S5) and is comparable to some of the most stable OSN membranes reported to date[18, 35, 53, 54]. This work also represents an unprecedented example of a polymer membrane whose OSN performance could be maintained extensively while a strongly acidic or basic organic solution is used as the feed. The chemical stability and robust porous structure of *p*-PPN membranes can be attributed to the rigid and inert aromatic nature of its backbone. The stable OSN performance of *p*-PPN in strong acid/base conditions not only makes it suitable for practical applications in these harsh environments, but also allows for treatment of the membranes with strong acid or base to tackle potential fouling problems.

Conclusions

In summary, aromatic PPN membranes were synthesized through a highly efficient ATC reaction using MSA as both the catalyst and the solvent, via simple drop-casting followed by *in situ* polymerization. These membranes can be fabricated from different monomers with controllable thicknesses. Despite their amorphous nature, the non-polar micropores are narrowly distributed in terms of sizes, enabling molecular-sieving effect in OSN with high intrinsic permeability and good selectivity. Benefiting from the aromatic framework, these PPN membranes exhibited outstanding thermal and chemical stability and consequently possess durable long-term OSN performance in either strong acid or strong base conditions. The combined merits of these membranes not only afford an outstanding potential OSN performance, but also provide opportunities to tackle the practical challenges in OSN in terms of extreme chemical conditions and membrane fouling.

Conflicts of interest

There are no conflicts to declare.

Acknowledgements

Notes and references

1. P. Marchetti, M. F. Jimenez Solomon, G. Szekely and A. G. Livingston, *Chem. Rev.*, 2014, **114**, 10735-10806.
2. P. Vandezande, L. E. M. Gevers and I. F. J. Vankelecom, *Chem. Soc. Rev.*, 2008, **37**, 365-405.
3. B. Liang, X. He, J. Hou, L. Li and Z. Tang, *Adv. Mater.*, 2018, 1806090.
4. G. Liu, W. Jin and N. Xu, *Angew. Chem. Int. Ed.*, 2016, **55**, 13384-13397.
5. R. P. Lively and D. S. Sholl, *Nat. Mater.*, 2017, **16**, 276-279.
6. Q. Yang, Y. Su, C. Chi, C. T. Cherian, K. Huang, V. G. Kravets, F. C. Wang, J. C. Zhang, A. Pratt, A. N. Grigorenko, F. Guinea, A. K. Geim and R. R. Nair, *Nat. Mater.*, 2017, **16**, 1198-1202.
7. J. Wang, P. Chen, B. Shi, W. Guo, M. Jaroniec and S.-Z. Qiao, *Angew. Chem. Int. Ed.*, 2018, **57**, 6814-6818.
8. C. Zhang, B.-H. Wu, M.-Q. Ma, Z. Wang and Z.-K. Xu, *Chem. Soc. Rev.*, 2019, **48**, 3811-3841.
9. X. Q. Cheng, Z. X. Wang, X. Jiang, T. Li, C. H. Lau, Z. Guo, J. Ma and L. Shao, *Prog. Mater. Sci.*, 2018, **92**, 258-283.
10. A. G. Livingston and R. Baker, *Nat. Mater.*, 2017, **16**, 280-282.
11. J. H. Kim, M. Cook, S. H. Park, S. J. Moon, J. F. Kim, A. G. Livingston and Y. M. Lee, *Green Chem.*, 2018, **20**, 1887-1898.
12. H. B. Park, J. Kamcev, L. M. Robeson, M. Elimelech and B. D. Freeman, *Science*, 2017, **356,** 10.1126/science.aab0530.
13. D. L. Gin and R. D. Noble, *Science*, 2011, **332**, 674-676.
14. Y. H. See Toh, F. W. Lim and A. G. Livingston, *J. Membr. Sci.*, 2007, **301**, 3-10.
15. Y. Li, S. Yuan, C. Zhou, Y. Zhao and B. Van der Bruggen, *J. Mater. Chem. A*, 2018, **6**, 22987-22997.
16. Q. Song, S. Jiang, T. Hasell, M. Liu, S. Sun, A. K. Cheetham, E. Sivaniah and A. I. Cooper, *Adv. Mater.*, 2016, **28**, 2629-2637.
17. P. Gorgojo, S. Karan, H. C. Wong, M. F. Jimenez‐Solomon, J. T. Cabral and A. G. Livingston, *Adv. Funct. Mater.*, 2014, **24**, 4729-4737.
18. S. Kandambeth, B. P. Biswal, H. D. Chaudhari, K. C. Rout, K. H. Shebeeb, S. Mitra, S. Karak, A. Das, R. Mukherjee, U. K. Kharul and R. Banerjee, *Adv. Mater.*, 2017, **29**, 1603945.
19. H. Fan, J. Gu, H. Meng, A. Knebel and J. Caro, *Angew. Chem. Int. Ed.*, 2018, **57**, 4083-4087.
20. D. B. Shinde, G. Sheng, X. Li, M. Ostwal, A.-H. Emwas, K.-W. Huang and Z. Lai, *J. Am. Chem. Soc.*, 2018, **140**, 14342-14349.
21. K. Dey, M. Pal, K. C. Rout, S. Kunjattu H, A. Das, R. Mukherjee, U. K. Kharul and R. Banerjee, *J. Am. Chem. Soc.*, 2017, **139**, 13083-13091.
22. M. Matsumoto, L. Valentino, G. M. Stiehl, H. B. Balch, A. R. Corcos, F. Wang, D. C. Ralph, B. J. Mariñas and W. R. Dichtel, *Chem*, 2018, **4**, 308-317.
23. S. Yuan, X. Li, J. Zhu, G. Zhang, P. Van Puyvelde and B. Van der Bruggen, *Chem. Soc. Rev.*, 2019, **48**, 2665-2681.
24. W. Lu, D. Yuan, D. Zhao, C. I. Schilling, O. Plietzsch, T. Muller, S. Bräse, J. Guenther, J. Blümel, R. Krishna, Z. Li and H.-C. Zhou, *Chem. Mater.*, 2010, **22**, 5964-5972.
25. D. Yuan, W. Lu, D. Zhao and H.-C. Zhou, *Adv. Mater.*, 2011, **23**, 3723-3725.
26. Y. Xu, S. Jin, H. Xu, A. Nagai and D. Jiang, *Chem. Soc. Rev.*, 2013, **42**, 8012-8031.

27. X. Zhu, C. Tian, S. Chai, K. Nelson, K. S. Han, E. W. Hagaman, G. M. Veith, S. M. Mahurin, H. Liu and S. Dai, *Adv. Mater.*, 2013, **25**, 4152-4158.
28. L. Ma, Y. Liu, Y. Liu, S. Jiang, P. Li, Y. Hao, P. Shao, A. Yin, X. Feng and B. Wang, *Angew. Chem. Int. Ed.*, 2019, **58**, 4221-4226.
29. S. N. Talapaneni, J. Kim, S. H. Je, O. Buyukcakir, J. Oh and A. Coskun, *J. Mater. Chem. A*, 2017, **5**, 12080-12085.
30. M. F. Jimenez-Solomon, Q. Song, K. E. Jelfs, M. Munoz-Ibanez and A. G. Livingston, *Nat. Mater.*, 2016, **15**, 760.
31. L. F. Villalobos, T. Huang and K. V. Peinemann, *Adv. Mater.*, 2017, **29**, 1606641.
32. J. Liu, D. Hua, Y. Zhang, S. Japip and T. S. Chung, *Adv. Mater.*, 2018, **30**, 1705933.
33. B. Liang, H. Wang, X. Shi, B. Shen, X. He, Z. A. Ghazi, N. A. Khan, H. Sin, A. M. Khattak, L. Li and Z. Tang, *Nat. Chem.*, 2018, **10**, 961-967.
34. X. He, H. Sin, B. Liang, Z. A. Ghazi, A. M. Khattak, N. A. Khan, H. R. Alanagh, L. Li, X. Lu and Z. Tang, *Adv. Funct. Mater.*, 2019, 1900134.
35. I. B. Valtcheva, S. C. Kumbharkar, J. F. Kim, Y. Bhole and A. G. Livingston, *J. Membr. Sci.*, 2014, **457**, 62-72.
36. K. H. Thebo, X. Qian, Q. Zhang, L. Chen, H.-M. Cheng and W. Ren, *Nat. Commun.*, 2018, **9**, 1486.
37. X. Guan, H. Li, Y. Ma, M. Xue, Q. Fang, Y. Yan, V. Valtchev and S. Qiu, *Nat. Chem.*, 2019, **11**, 587-594.
38. X. Wu, G. Zhou, X. Cui, Y. Li, J. Wang, X. Cao and P. Zhang, *ACS Appl. Mater. & Interfaces*, 2019, **11**, 17804-17813.
39. M.-L. Liu, J.-L. Guo, S. Japip, T.-Z. Jia, D.-D. Shao, S. Zhang, W.-J. Li, J. Wang, X.-L. Cao and S.-P. Sun, *J. Mater. Chem. A*, 2019, **7**, 3170-3178.
40. Z.-H. Guo, C. Wang, Q. Zhang, S. Che, H.-C. Zhou and L. Fang, *Mater. Chem. Front.*, 2018, **2**, 396-401.
41. S.-M. Jung, J. Park, D. Shin, H. Y. Jeong, D. Lee, I.-Y. Jeon, H. Cho, N. Park, J.-W. Yoo and J.-B. Baek, *Angew. Chem. Int. Ed.*, 2019, 10.1002/anie.201903226.
42. S. Luque, D. Gómez and J. R. Álvarez, *Membr. Sci. Technol.*, 2008, **13**, 177-216.
43. T. Yao, S. Guo, C. Zeng, C. Wang and L. Zhang, *J. Hazard. Mater.*, 2015, **292**, 90-97.
44. Y. Miyah, A. Lahrichi, M. Idrissi, A. Khalil and F. Zerrouq, *Surf. Interfaces*, 2018, **11**, 74-81.
45. A. A. Alqadami, M. Naushad, Z. A. Alothman and T. Ahamad, *J. Environ. Manage.*, 2018, **223**, 29-36.
46. J. G. Wijmans and R. W. Baker, *J. Membr. Sci.*, 1995, **107**, 1-21.
47. B. Li, Y. Cui, S. Japip, Z. Thong and T.-S. Chung, *Carbon*, 2018, **130**, 503-514.
48. L. M. Robeson, *J. Membr. Sci.*, 1991, **62**, 165-185.
49. L. M. Robeson, *J. Membr. Sci.*, 2008, **320**, 390-400.
50. G. M. Shi, M. H. A. Farahani, J. Y. Liu and T.-S. Chung, *J. Membr. Sci.*, 2019, **588**, 117202.
51. M. Bastin, K. Hendrix and I. Vankelecom, *J. Membr. Sci.*, 2017, **536**, 176-185.
52. K. Werth, P. Kaupenjohann, M. Knierbein and M. Skiborowski, *J. Membr. Sci.*, 2017, **528**, 369-380.
53. L. Huang, J. Chen, T. Gao, M. Zhang, Y. Li, L. Dai, L. Qu and G. Shi, *Adv. Mater.*, 2016, **28**, 8669-8674.
54. C. Chen, J. Wang, D. Liu, C. Yang, Y. Liu, R. S. Ruoff and W. Lei, *Nat. Commun.*, 2018, **9**, 1902.